Title

Restraint of melanoma progression by cells in the local skin environment

Authors

Yilun Ma[1-3], Mohita Tagore[2], Miranda V. Hunter[2], Ting-Hsiang Huang[2], Emily Montal[2], Joshua M. Weiss[1-3], Richard M. White[2,4]

Affiliations

[1] Weill Cornell/Rockefeller/Sloan Kettering Tri-Institutional MD-PhD Program, New York, NY, USA

[2] Department of Cancer Biology and Genetics, Memorial Sloan Kettering Cancer Center, New York, NY, USA

[3] Cell and Developmental Biology Program, Weill Cornell Graduate School of Medical Sciences, New York, NY, USA

[4] Nuffield Department of Medicine, Ludwig Cancer Research, University of Oxford, Oxford, UK

Abstract

Keratinocytes, the dominant cell type in the melanoma microenvironment during tumor initiation, exhibit diverse effects on melanoma progression. Using a zebrafish model of melanoma and human cell co-cultures, we observed that keratinocytes undergo an Epithelial–Mesenchymal Transition (EMT)-like transformation in the presence of melanoma, reminiscent of their behavior during wound healing. Surprisingly, overexpression of the EMT transcription factor Twist in keratinocytes led to improved overall survival in zebrafish melanoma models, despite no change in tumor initiation rates. This survival benefit was attributed to reduced melanoma invasion, as confirmed by human cell co-culture assays. Single-cell RNA-sequencing revealed a unique melanoma cell cluster in the Twist-overexpressing condition, exhibiting a more differentiated, less

26 invasive phenotype. Further analysis nominated homotypic jam3b-jam3b and pgrn-sort1a
27 interactions between Twist-overexpressing keratinocytes and melanoma cells as potential
28 mediators of the invasive restraint. Our findings suggest that EMT in the tumor microenvironment
29 (TME) may limit melanoma invasion through altered cell-cell interactions.
30

31 ## Introduction

32 The complex interplay between cancer cells and their microenvironment has emerged as a critical
33 determinant of tumor progression and therapeutic response. In melanoma, the tumor
34 microenvironment (TME) encompasses diverse cell types, including immune cells, fibroblasts,
35 and endothelial cells[1]. However, during melanoma initiation the dominant cell type in the TME is
36 the keratinocyte, an epithelial cell which makes up the majority of our skin surface. In normal
37 homeostasis, each melanocyte reciprocally interacts with 30-40 keratinocytes[2], and this
38 interaction is essential for skin and hair color[3,4]. Despite decades of research, our understanding
39 of keratinocytes in the context of melanoma remains incomplete.

40 Keratinocytes have been shown to both inhibit and promote melanoma initiation. They are tightly
41 adherent to melanocytes through homophilic interactions of the cell adhesion molecule E-
42 cadherin[5]. Through E-cadherin, keratinocytes can control melanocyte growth and behavior[6–9]. As
43 melanoma progresses, they undergo a cadherin subtype switch in which they downregulate E-
44 cadherin and upregulate N-cadherin, thereby escaping keratinocyte-mediated controls while
45 promoting migration and survival[10–12]. Beyond cadherins, invasive melanoma can downregulate
46 matricellular proteins such as CCN3, which usually facilitates melanoma attachment to the
47 basement membrane[13,14]. In addition to melanoma intrinsic changes, alterations in epidermal
48 keratinocytes such as the loss of PAR3 expression results in a local environment that facilitates
49 melanoma invasion and metastasis[15]. In contrast, keratinocytes can also promote tumor

development through secretion of growth factors such as endothelins or via GABAergic crosstalk between the two cell types[16–18].

These conflicting data highlight that interactions between keratinocytes and nascent melanoma cells are likely dynamic and change rapidly during tumor initiation. Studying the nature of these interactions in human samples is challenging because biopsies are taken after the patient has come to the clinic, meaning that the earliest interactions in tumor initiation will be missed. This necessitates models which faithfully recapitulate the earliest stages of tumor initiation, yet have the cellular resolution to measure interactions between melanoma cells and keratinocytes.

In this study, we utilized a zebrafish model of melanoma to investigate the earliest interactions between melanoma cells and their neighboring keratinocytes[19]. Zebrafish have emerged as a powerful tool for cancer research due to their genetic tractability, conserved biology, and the ability to visualize tumor development and progression in real-time within the context of an intact organism[20,21]. Using a combination of cell-type specific genetic manipulations, in vivo imaging, and single-cell transcriptomics, we found that tumor-associated keratinocytes undergo changes associated with EMT, similar to what is found in wounded skin. Unexpectedly, we found that this keratinocyte EMT suppresses melanoma progression. This change in the keratinocytes occurs shortly after melanoma initiation, and results in keratinocytes which are more adhesive to these nascent tumor cells and prevents their movement out of the epidermis. Our data suggests that melanoma initiation revises an evolutionarily conserved wounding response in the nearby skin environment, which acts as a cell extrinsic tumor suppressor to prevent newly transformed cells from becoming clinically meaningful.

Results

Melanoma initiation is associated with EMT in keratinocytes

74 To investigate the relationship between keratinocytes and melanoma cells *in vivo*, we created a
75 transgenic zebrafish line in which GFP is expressed under the *krt4* promoter[22]. This line faithfully
76 marks all adult keratinocytes present throughout the fish epidermis and scales, similar to previous
77 lines using this promoter (Figure 1A). We then initiated melanomas in this background using the
78 TEAZ method (Transgene Electroporation in Adult Zebrafish)[19,23], in which plasmids containing
79 oncogenes or sgRNAs against tumor suppressors can be introduced directly into the skin (Figure
80 1B). The major advantage of this method is that we can visualize melanoma initiation when the
81 tumor is in its early stages, consisting of a small number of cells. We initiated tumors with a
82 combination of $BRAF^{V600E}$, sgRNAs against PTEN (zebrafish *ptena/b)* and germline loss of p53,
83 using *mitfa*-Cas9 to ensure that *PTEN* were inactivated only in melanocytes and not in
84 surrounding skin cells (Figure 1C). To account for skin wounding from electroporation in
85 assessing changes in tumor-associated keratinocytes, we also performed TEAZ using a control
86 vector that labels melanocyte-precursors but does not induce melanoma formation. Fluorescent
87 imaging 8-weeks post-electroporation with the control vector demonstrated an injury-free
88 epidermis, in contrast to the pronounced melanoma development in zebrafish administered with
89 the oncogenic vectors (Figure 1D).

90 After initiating tumorigenesis, we examined the morphology of tumor-adjacent keratinocytes to
91 investigate whether the growing tumor could be influencing keratinocyte behavior. We performed
92 confocal microscopy on the scales of fish 8 weeks post-electroporation. This revealed a marked
93 disruption of keratinocyte morphology in the tumor bearing fish, which was not seen in control
94 fish. We specifically noted disrupted cell-cell junctions, a disorganized pattern of keratinocytes,
95 and loss of the normal hexagonal cell layer (Figure 1E). These changes were reminiscent of
96 keratinocyte EMT, which has been previously noted to occur in wounded epidermis[24–26]. To further
97 assess this possibility, we excised tissues from both tumor and control skin and used FACS to
98 isolate keratinocytes (GFP+) and melanoma cells (tdTomato+) and performed qPCR (Figure 1B).

99 As expected, we found enrichment of *mitfa* in melanoma cells and *krt4* in keratinocytes, validating
100 the successful cell-type isolation (Figure 1F). Comparative analyses between tumor-associated
101 keratinocytes (TAKs) and normal keratinocytes (NKCs) from tissue without melanoma revealed
102 upregulation of EMT markers vimentin and N-cadherin in TAKs, confirming the EMT-like
103 morphological changes of keratinocytes in our imaging results (Figure 1G).

104 We next asked whether these changes were also seen in human samples. To address this, we
105 performed co-culture experiments between keratinocytes and melanoma cells. We grew GFP-
106 labeled HaCaT keratinocytes either alone or with A375 melanoma cells for 21 days, followed by
107 isolation by FACS for bulk RNA-sequencing as published in Tagore et al.[18] (Figure 1H). Consistent
108 with our *in vivo* results in the fish, the top pathway altered in the co-cultured HaCaT cells was
109 enrichment of EMT (Figure 1I). Differential gene expression analysis showed notable upregulation
110 of the mesenchymal markers vimentin and N-cadherin in co-cultured keratinocytes compared to
111 monocultured control keratinocytes (Figure 1J), similar to what was found in vivo. Collectively, our
112 data indicate that melanoma cells induce morphological and molecular markers of EMT in nearby
113 keratinocytes.
114

115 **EMT transcription factors are upregulated in tumor-associated keratinocytes**

116 EMT is usually driven by upstream transcription factors, which then act on downstream targets to
117 repress adhesion molecules such as E-cadherin or activate other adhesion molecules such as N-
118 cadherin[26]. We next wanted to understand which of these transcription factors was responsible
119 for the EMT-like behavior in tumor-associated keratinocytes. To address this, we utilized an
120 existing scRNA-sequencing dataset of a $BRAF^{V600E}$-driven zebrafish melanoma[27] (Figure 2A).
121 Dimensionality reduction with UMAP and subsequent clustering revealed two keratinocyte
122 populations as indicated by module scoring for genes enriched in zebrafish keratinocyte
123 populations (Figure 2B). Subsequent differential gene expression and GSEA analysis of the two

124 keratinocyte clusters revealed one cluster with enrichment for EMT, similar to what we observed
125 in Figure 1 (Figure 2C-D). We refer to this EMT cluster as Tumor Associated Keratinocytes
126 (TAKs), and the other cluster as a Normal Keratinocyte Cluster (NKCs). We focused on three
127 EMT-transcription factors expressed by zebrafish keratinocytes in this dataset, *snai1a*, *snai2*,
128 *twist1a*, zebrafish homologs of human SNAIL, SLUG and TWIST. Differential expression showed
129 significant enrichment in *snai1a* and *twist1a* in TAK vs. NKC clusters (Figure 2F). The significant
130 enrichment of *twist1a* in the TAK cluster, coupled with its rare expression in NKCs, positioned
131 *twist1a* as a promising candidate for further investigation into its potential role in driving EMT-like
132 changes in keratinocytes and, consequently, its impact on melanoma progression.
133

134 **Keratinocyte *TWIST* restrains melanoma invasion in zebrafish**

135 Having identified Twist as a potential driver of EMT-like changes in tumor-associated
136 keratinocytes, we next asked how it affected melanoma phenotypes. To investigate the role of
137 Twist in keratinocytes, we created new transgenic zebrafish in which the keratinocyte-specific *krt4*
138 promoter was used to drive the two zebrafish *TWIST* paralogs (*twist1a* and *twist1b*) in the
139 presence of BRAF^{V600E}-driven melanomas. We injected the plasmids for melanoma initiation to
140 zebrafish embryos and then monitored the fish for tumor-free survival as well as overall survival
141 over the ensuing 26 weeks (Figure 3A). Interestingly, we found no difference in melanoma
142 initiation rate in the TWIST overexpression condition compared to empty vector (Figure 3B).
143 Unexpectedly, however, we noted that overall survival was improved in the transgenic animals
144 expressing TWIST in the keratinocytes (Figure 3B).

145 This discrepancy between melanoma-free and overall survival suggested that the tumors in the
146 TWIST condition should be phenotypically distinct from the control tumors. To assess this, we
147 performed immunohistochemistry on the tumors and surrounding tissues from the control and
148 TWIST conditions (Figure 3C). The oncogenic driver in this melanoma model is hBRAF^{V600E} and

149 serves as an IHC marker for the tumor cells. Comparison of hBRAF^{V600E} staining revealed
150 significant melanoma infiltration into the zebrafish body in the CTRL condition, as opposed to a
151 nearly non-invasive tumor in the TWIST condition (Figure 3D). The lack of melanoma invasion
152 was also observed when the melanoma developed in other anatomical locations (Supp. Figure
153 1). These findings suggest that *twist1a/twist1b* overexpression in keratinocytes does not impair
154 tumor initiation, but instead impairs melanoma invasion and improves survival when expressed in
155 the microenvironment.

156 To further validate this finding, we developed a cell culture-based invasion assay by pairing the
157 HaCaT keratinocyte cell line with multiple melanoma cell lines that were pre-cultured on coverslips
158 (Figure 4A). Due to the migratory nature of melanoma cells, they will migrate off the coverslip and
159 infiltrate the layer of keratinocytes, allowing us to assess relative differences between culture
160 conditions. HaCaT keratinocytes were transformed via lentiviral transduction to overexpress
161 human *TWIST1* (HaCaT-TWIST) or an empty vector control (HaCaT-CTRL) (Figure 4B). Western
162 blot analysis confirmed robust Twist protein overexpression in HaCaT-TWIST compared to
163 HaCaT-CTRL (Figure 4C), and immunofluorescence imaging revealed nuclear localization of
164 Twist (Figure 4D). Co-culture of HS294T melanoma cells with HaCaT-TWIST resulted in
165 significantly reduced melanoma cell invasion into keratinocytes compared to HaCaT-CTRL
166 (Figure 4E-F), similar to what we had observed *in vivo*. This finding was recapitulated using the
167 SKMEL2 human melanoma cell line, demonstrating the inhibitory effect of *TWIST1*
168 overexpression in keratinocytes on melanoma invasion across different cell lines (Figure 4G-H).
169 Collectively, our results demonstrate that induction of EMT in keratinocytes is associated with
170 reduced melanoma invasion and improvement in animal survival.

171

172 **Keratinocyte EMT promotes aberrant adhesion to nascent melanoma cells**

173 While EMT of tumor cells is well recognized to promote invasion, our data suggest that EMT in
174 the microenvironment paradoxically restrains tumor invasion. We wanted to better understand the
175 downstream mechanisms accounting for this result. We therefore analyzed our CTRL vs. TWIST
176 overexpression tumors and adjacent microenvironment using single-cell RNA sequencing, which
177 would allow us to understand potential mechanisms by which melanoma cells were interacting
178 with these keratinocytes. Melanoma and adjacent skin from three fish per condition (CTRL or
179 TWIST) were dissociated into single cell suspensions and FACS-sorted for eGFP+ keratinocytes
180 and tdTomato+ melanoma cells (Figure 5A and Supp Figure 2A). In the resultant scRNA-seq
181 dataset, we identified distinct clusters of eGFP+ keratinocytes and tdTomato+ melanoma cells
182 (Figure 5B). Of the keratinocyte clusters identified, two were present in both the CTRL and TWIST
183 conditions, while a third was only present in samples overexpressing TWIST in keratinocytes
184 (Figure 5C). To identify biological processes that may be active within the keratinocyte, we
185 performed GSEA, comparing differentially expressed genes between the two clusters present in
186 both conditions. GSEA identified an enrichment in the EMT pathway as seen in Figure 2, allowing
187 us to label the EMT-enriched cluster as TAK and other as NKC (Figure 5D and Supp Figure 2B).
188 As expected, we also identified a unique cluster of keratinocytes only present in the TWIST
189 dataset that highly expresses *twist1a/b*, the genes that we overexpressed in the TWIST condition,
190 and labeled this cluster Twist-High (Figure 5D and Supp Figure 2C).

191 To understand how the Twist-high keratinocytes may be restraining melanoma progression, we
192 compared gene expression in melanomas that arose in the presence of control vs. Twist
193 overexpression keratinocytes by comparing their gene signatures to published melanoma gene
194 signatures representing a range of differentiation states[28]. It is now widely recognized that
195 melanoma cells exist along a trajectory of differentiation, ranging from undifferentiated/invasive,
196 to neural crest, to intermediate, to melanocytic/proliferative[28]. Interestingly, we found a cluster of
197 melanoma cells that developed in the TWIST condition was enriched for the

198 melanocytic/proliferative state but not undifferentiated/invasive gene markers (Figure 5E). This is
199 consistent with our in vivo observations that these melanomas are phenotypically less invasive.

200 We hypothesized that this change in cell state might be induced by physical interactions between
201 the Twist-high keratinocytes and the melanoma cells. To address this, we analyzed potential cell-
202 cell interactions using CellChat, a software tool that allows us to quantitatively characterize and
203 visualize cell-cell communications using a curated zebrafish ligand-receptor interaction
204 database[29] (Figure 5F). Two unique ligand-receptor pairings were identified that only occur
205 between Twist-high keratinocytes and the melanomas that arose in these animals: a homophilic
206 *jam3b-jam3b* interaction and a *pgrn-sort1a* (progranulin-sortilin) interaction (Figure 5G).

207 The *jam3b* interaction was of particular interest to us, as this protein has been recently identified
208 as one required for melanophore survival in zebrafish[30] and for human melanoma metastasis[31,32].
209 In normal human skin, JAM1 (or F11R) is expressed in keratinocytes of the superficial epidermis,
210 whereas its heterophilic partner JAM3 is exclusively found in basal keratinocytes[33,34]. This
211 distribution is significant because melanomas predominantly originate in the basal area of the
212 skin. Interestingly, basal keratinocytes, but not superficial keratinocytes, have been shown to
213 inhibit melanocyte growth[7]. This observation, combined with our findings, suggests that Twist
214 expression in the keratinocytes was leading to aberrant expression of jam3b, resulting in stronger
215 homophilic jam3b-jam3b attachments between these keratinocytes and melanoma cells,
216 potentially inhibiting melanoma invasion.
217

218 ## Discussion

219 In this study, we observed that keratinocytes in both zebrafish and human models of melanoma
220 undergo an EMT-like transformation in the presence of melanoma. This alteration is reminiscent
221 of keratinocyte behavior during wound healing, in which keratinocytes exhibit markers and

222 morphological changes associated with EMT in development[25,35]. Interestingly, we observed an
223 increase in N-cadherin expression in KC, which is usually attributed to melanoma as it becomes
224 more aggressive and invades into the dermis to associate with fibroblasts[10]. Our findings would
225 suggest a subpopulation of keratinocytes could maintain contact with melanoma through
226 upregulation of N-cadherin. Additionally, re-analysis of a published zebrafish melanoma scRNA-
227 sequencing dataset showed distinct populations of keratinocytes that expressed markers of
228 EMT, demonstrating the feasibility of studying this KC population using our zebrafish model and
229 nominating Twist1 as a potent EMT transcription factor in this cell type[27]. Twist expression has
230 been found to be upregulated at the edge of wounded skin upon treatment with bFGF, a well-
231 characterized growth factor produced by melanoma[35,36]. If melanoma acts as an open-wound in
232 the skin, then Twist1 might be upregulated in tumor-associated keratinocytes as an adaptive
233 response to close this wound.
234
235 Our zebrafish melanoma survival experiment showed improvements in overall survival in
236 zebrafish with keratinocytes overexpressing Twist compared to those that received an empty
237 vector, despite the fish forming tumors at the same rate. This survival improvement was shown
238 to be caused by a decrease in melanoma invasion, raising the possibility that Twist
239 overexpressing keratinocytes could restrain melanoma invasion. Human cell co-cultures with a
240 HaCaT cell line overexpressing Twist showed a similar finding to our in vivo zebrafish model,
241 with reduced melanoma cell infiltration into keratinocytes. To learn more about the dynamics of
242 melanoma and TME keratinocytes, we performed scRNA-sequencing on our zebrafish
243 melanoma model to account for both keratinocytes in contact with melanoma and those in the
244 periphery. Compared to the fish that received an empty vector control that had two
245 subpopulations of keratinocytes, fish with Twist overexpression contained an additional novel
246 keratinocyte subpopulation with overexpression of *twist1a/b*[27].
247

248 Interestingly, we also found a cluster of melanoma cells unique to the TWIST condition, which
249 shared gene signatures similar to that of the genes observed in both transitory and melanocytic
250 states as published by Tsoi et al.[28]. These cell states were defined to be more differentiated with
251 higher MITF expression and correlated to a more proliferative but less invasive cohort from
252 Hoek et al.[37]. The enrichment for specific melanoma cell states when surrounded by a Twist-
253 overexpressing keratinocyte TME could be responsible for the reduced overall melanoma
254 invasion.
255
256 Further analysis using CellChat nominated *jam3b-jam3b* and *pgrn-sort1a* as unique interactions
257 between Twist-High keratinocytes and TWIST-Melanoma cells. As previously described, jam3b
258 has been identified as a critical protein in zebrafish melanophore survival with known
259 involvement in melanoma metastasis[30]. The aberrant expression of jam3b on Twist-
260 overexpressing keratinocytes could indicate strong homophilic interactions with melanoma
261 jam3b that retains the melanoma in the epidermis. Whether jam3b acts in concert or
262 independent of cadherin-based adhesion remains to be determined in future studies. Although
263 the progranulin-sortilin interaction has not been characterized in melanoma, sortilin has been
264 identified as a key regulator of progranulin levels[38]. Progranulin is known to be constitutively
265 expressed by keratinocytes, which could be cleaved to epithelins that promote KC
266 proliferation[39,40]. Progranulin is also a potent mediator of the wound response produced by
267 dermal fibroblasts in addition to epidermal keratinocytes[41]. Perhaps the increase in progranulin
268 is cleared by melanoma cells through sortilin, resulting in the endocytosis and lysosomal
269 transport of sortilin[42]. The degradation of sortilin could be responsible for decreased cell
270 migration and invasion, as sortilin is required for the interaction of proNGF, a neurotrophin
271 produced by melanoma, with NGFR in promoting melanoma migration[43]. Further studies are
272 needed to elucidate the precise mechanisms underlying the nominated interactions, jam3b-
273 jam3b and pgrn-sort1a, and to explore their potential as therapeutic targets in melanoma.

274

275 ## Methods

276 **Zebrafish husbandry**

277 Zebrafish were maintained in a dedicated facility with controlled temperature (28.5 °C) and
278 salinity. The fish were kept on a 14-hour light/10-hour dark cycle and fed a standard zebrafish
279 diet consisting of brine shrimp followed by Zeigler pellets. Embryos were obtained through
280 natural mating and incubated in E3 buffer (5 mM NaCl, 0.17 mM KCl, 0.33 mM $CaCl_2$, 0.33 mM
281 $MgSO_4$) at 28.5 °C. For procedures requiring immobilization, zebrafish were anesthetized using
282 Tricaine-S (MS-222, Syndel) prepared as a 4 g/L stock solution with a pH of 7.0. The stock
283 solution was protected from light exposure and diluted to the appropriate concentration to
284 achieve fish immobilization. All experimental procedures and animal protocols described in this
285 manuscript were conducted in compliance with the Institutional Animal Care and Use
286 Committee (IACUC) protocol #12-05-008, approved by the Memorial Sloan Kettering Cancer
287 Center (MSKCC).

288

289 **Generation of zebrafish line with fluorophore labeled keratinocytes**

290 Embryos at the one-cell stage from the Casper Triple zebrafish line (*mitfa:BRAF^{V600E};p53-*
291 */-;mitfa-/-;mpv17-/-*)[19,44] were injected with a *krt4:eGFP* expression cassette in the 394 vector of
292 the Tol2Kit[45] with tol2 mRNA. Larvae were sorted for positive GFP fluorescence at day 3 and
293 raised to adult for breeding. F0 fish were in-crossed and resulting F1 were outcrossed with
294 Casper Triple zebrafish for consistent GFP expression. Starting from F2, the *krt4:eGFP*
295 zebrafish line was maintained by out-crossing with Casper Triple zebrafish and sorting for GFP
296 expression.

297

298 **Transgene Electroporation in Adult Zebrafish (TEAZ)**

299 TEAZ was utilized to generate melanoma as previously described[19,46]. *Krt4:eGFP* zebrafish
300 (*krt4:eGFP* Casper Triple) were anesthetized with tricaine and injected with a plasmid solution
301 containing miniCoopR-tdT (250ng/µl), mitfa:Cas9 (250 ng/µl); *zU6:sgptena* (23 ng/µl),
302 *zU6:sgptenb* (23ng/µl), and the tol2 plasmid (55ng/µl). For control electroporation without
303 generating melanoma, zebrafish were injected with *mitfa:tdTomato* (250ng/µl), *mitfa:*Cas9 (250
304 ng/µl), *zU6:*non-targeting (46ng/µl) and tol2 plasmid (55ng/µl). All fish were injected on the left
305 flank below the dorsal fin and electroporated with the BTX ECM 830 electroporator using 3mm
306 platinum Tweezertrodes (BTX Harvard Apparatus; #45-0487). Electroporator settings used: LV
307 Mode, 40V, 5 pulses, 60ms pulse length, and 1s pulse interval. Electroporated zebrafish were
308 screened for successful electroporation 7 days post-electroporation by tdTomato expression
309 using fluorescence microscopy and melanoma tracked by imaging once per week. All live
310 zebrafish imaging were performed with the Zeiss AxioZoom V16 fluorescence microscope.
311
312 sgRNA sequences for TEAZ listed below:
313 Nontargeting: 5'-AACCTACGGGCTACGATACG-3'
314 ptena: 5'-GAATAAGCGGAGGTACCAGG-3'
315 ptenb: 5'-GAGACAGTGCCTATGTTCAG-3'
316
317 **Confocal imaging of zebrafish epidermis**
318 Zebrafish with or without melanoma were anesthetized in tricaine (MS-222, Syndel) as
319 described above. Site of injection is visually identified by the presence of melanoma or the area
320 below the dorsal fin. Scales were removed with tweezers and fixed in 4% PFA in PBS (Santa
321 Cruz 281692) in a 96-well plate for 15 minutes. Fixed scales were washed three times with PBS
322 and permeabilized with 0.1% Triton-X 100 (Thermo Scientific 85111) in PBS, then blocked with
323 10% goat serum (Thermo Fisher 50062Z). Scales were incubated with 1:250 GFP polyclonal
324 antibody, Alexa Fluor 488 (Thermo Fisher A21311) overnight at 4°C. Next day, scales were

325 washed three times with PBS, incubated with 1:1000 Hoechst 33342 (Thermo Fisher H3570) for
326 1 hour and mounted onto slides with VECTASHIELD Vibrance Antifade Mounting Media (Vector
327 Laboratories H-1700). Samples were imaged on the Zeiss LSM880 inverted confocal
328 microscope and images were processed using FIJI v1.53.
329
330 **Flow cytometry of adult zebrafish cells**
331 Zebrafish were euthanized using ice-cold water. Melanoma and adjacent skin were dissected
332 from fish with melanoma and skin alone was dissected from below the dorsal fin. Subsequently,
333 samples were cut into 1mm strips using a clean scalpel and placed into 15 mL conical tubes
334 (Falcon 352099) with 3 ml of DPBS (Gibco 14190250) and 187.5µl of 2.5 mg/ml Liberase TL
335 (Roche 5401020001). Samples were incubated in dissociation solution at room temperature for
336 30 minutes on a shaker with gentle movement to prevent tissue from settling at the bottom of
337 the tube. At 15 minutes of incubation, a wide bore p1000 pipette tip (Thermo Scientific 2079G)
338 was used to gently pipette the sample up and down for 90 seconds. After 30 minutes, 250 µl of
339 FBS (Gemini Bio) was added to stop the enzymatic activity of Liberase TL and samples were
340 pipetted up and down using a wide bore p1000 pipette tip for 90 seconds. Dissociated cells
341 were then filtered through a 70 µm cell strainer (Falcon 352350) into a 50 mL conical tube
342 (Falcon 352098) placed on ice. Samples were centrifuged at 500g at 4°C for 5 minutes and
343 supernatant was removed by pipetting. The cell pellet was resuspended in 500 µl of PBS with
344 5% FBS and filtered again through 40 µm tip filters (Bel-Art H136800040) into 5 ml
345 polypropylene tubes (Falcon 352063). For subsequent FACS analysis, 0.5 µl of 1000x DAPI
346 (Sigma-Aldrich D9542) was added to each sample. Samples were FACS sorted (BD FACSAria)
347 at 4°C for GFP-positive keratinocytes and tdTomato-positive melanoma gated using
348 fluorophore-negative zebrafish controls.
349
350 **Zebrafish tissue RNA extraction and real-time quantitative PCR (RT-qPCR)**

351 FACS sorted zebrafish cells were deposited directly into 750 µl TRIzol LS Reagent (Invitrogen
352 10296010) in Eppendorf DNA LoBind Tubes (Eppendorf 022431021). After collection, samples
353 were snap-frozen using dry ice and stored at -80°C. RNA extraction was performed per TRIzol
354 LS manufacturer protocols. For precipitation of RNA, 10ug supplemental glycogen (Roche
355 10901393001) was used per sample to account for low cell numbers. Resulting RNA was
356 resuspended in Nuclease-free water (Fisher Scientific AM9937). 25ng RNA per sample was
357 transcribed to cDNA using Superscript III First-Strand Synthesis System (Invitrogen 18080051).
358 cDNA mix was diluted 1:10 with Nuclease free water for RT-qPCR using Power SYBR Green
359 PCR Master Mix (Applied Biosystems 4368708) and the Bio-Rad CFX384 Touch Real-Time
360 PCR System (Bio-Rad 1855484). Resulting Cq values were normalized to *hatn10* as previously
361 described.
362
363 qPCR primer sequences:
364 *hatn10* fwd: 5'- TGAAGACAGCAGAAGTCAATG-3′
365 *hatn10* rev: 5′-CAGTAAACATGTCAGGCTAAATAA-3′
366 mitfa fwd: 5'-GGCACCATCAGCTACAATGA-3'
367 mitfa rev: 5'-GAGACAGGGTGTTGTCCATAAG-3'
368 krt4 fwd: 5'-GGAGGTGTTTCCTCTGGTTATG-3'
369 krt4 rev: 5'-GAACCGAATCCTGATCCACTAC-3'
370 vim fwd: 5'-GGATATTGAGATCGCCACCTAC-3'
371 vim rev: 5'-GACTCTCGCAGGCTTAATGAT-3'
372 cdh2 fwd: 5'-GAGCCATCATCGCCATACTT-3'
373 cdh2 rev: 5'-CTTGGCCTGTCTCTCTTTATCC-3'
374
375 **Re-analysis of zebrafish scRNA-sequencing data from Hunter et al.**

376 Zebrafish scRNA-seq data from ref[27] was re-analyzed using R 4.2.0. and Seurat 4.3.0[47,48].
377 Cluster identities were maintained as published. Keratinocyte Module Scores were calculated
378 using the AddModuleScore function with default parameters using published gene lists.
379 Differential Gene Expression (DGE) analyses between clusters were performed using
380 FindMarkers. Differentially expressed gene lists were converted from zebrafish genes to human
381 orthologs using DIOPT as previously described[49,50]. GSEA analysis on differentially expressed
382 genes between keratinocyte clusters was performed using fgsea 1.22.0 and the Hallmark
383 pathways set from MSigDB[51,52].
384
385 **Twist overexpression in zebrafish keratinocytes**
386 *Twist1a* (ENSDART00000043595.5) and *twist1b* (ENSDART00000052927.7) were TOPO
387 cloned into the attL1-L2 Gateway pME vector and LR cloned into the pDestTol2pA2 vector
388 (Tol2Kit 394) with p5E-*krt4* promoter and p3E-polyA (Tol2Kit 302). To generate the zebrafish
389 melanoma model as previously described, one-cell stage Casper Triple zebrafish embryos
390 (*mitfa:BRAF^{V600E};p53-/-;mitfa-/-;mpv17-/-*) were injected with miniCoopR-tdTomato, *krt4-eGFP*,
391 either *krt4-twist1a* and *krt4-twist1b* for Twist overexpression condition or empty vector for control
392 condition, tol2 mRNA and phenyl red. Injections were performed three times on different days
393 with parents from the same clutch. Embryos were grown at standard conditions and sorted at 5
394 days post-injection for eGFP and tdTomato expression using the Zeiss AxioZoom V16
395 fluorescence microscope. eGFP+/tdTomato+ fish in the CTRL (n=135) and TWIST (n=118)
396 conditions were maintained to adulthood.
397
398 **Zebrafish imaging and tumor-free survival tracking**
399 Zebrafish were regularly monitored for melanoma formation and survival every 4 weeks,
400 beginning at 10 weeks post-fertilization. Melanoma formation was screened visually using the
401 Zeiss AxioZoom V16 fluorescence microscope under 20X magnification. Kaplan-Meier curves

402 and corresponding statistics were generated using GraphPad Prism 9. Statistical differences in
403 survival between conditions were determined by the Mantel-Cox log-rank test.
404
405 **Histology of zebrafish samples**
406 Zebrafish were euthanized in tricaine (MS222, Syndel). Each fish was dissected in three
407 sections consisting of head, body, and tail. Samples were placed in 4% PFA in PBS (Santa
408 Cruz 281692) for 72h on a shaker at 4°C, then paraffin embedded. Histology was performed by
409 HistoWiz Inc. (histowiz.com). Samples were processed, embedded in paraffin, and sectioned at
410 5µm. Immunohistochemistry was performed on a Bond Rx autostainer (Leica Biosystems) with
411 enzyme treatment (1:1000) using standard protocols. Sections were stained with H&E or IHC
412 with antibodies including BRAFV600E (ab228461) and GFP (ab183734). Bond Polymer Refine
413 Detection (Leica Biosystems) was used according to the manufacturer's protocol. After staining,
414 sections were dehydrated and film coverslipped using a TissueTek-Prisma and Coverslipper
415 (Sakura). Whole slide scanning (40x) was performed on an Aperio AT2 (Leica Biosystems).
416
417 **Cell culture**
418 Human melanoma lines A375, HS294T, and SKMEL2 were obtained from ATCC. Human
419 keratinocyte line HaCaT was obtained from AddexBio. All cells were routinely tested and
420 confirmed to be free from mycoplasma. Cells were maintained in a humidified incubator at 37°C
421 and 5% CO2. Cells were maintained in DMEM (Gibco 11965) supplemented with 10% FBS
422 (Gemini Bio) and split when confluent, approximately 2-3 times per week.
423
424 **Twist overexpression in HaCaT**
425 The HaCaT cell line was labeled with eBFP to allow for identification during co-culture. 293T
426 (ATCC) was transfected with the pLV-Azurite plasmid (Addgene 36086) with pMD2.5 (Addgene
427 12259) and psPAX2 (Addgene 12260) using Invitrogen Lipofectamine 3000 Transfection

428 Reagent (Invitrogen L3000015) according to manufacturer protocol. HaCaTs were infected with
429 lentivirus containing *CMV:eBFP* and selected for eBFP positivity using ampicillin and FACS.
430 Subsequently, HaCaT-eBFP was infected with lentivirus containing *CMV:TWIST1* (Horizon
431 Precision LentiORF Human TWIST1 OHS5898-202622685) or *CMV:*empty control created by
432 removing ORF of *CMV:TWIST1* plasmid. HaCaT line overexpressing *TWIST1* was labeled as
433 HaCaT-TWIST and HaCaT line with empty vector was labeled as HaCaT-CTRL. HaCaT lines
434 were subsequently sorted for nuclear eGFP expression present in the plasmid as part of the
435 Precision LentiORF system. HaCaT-CTRL and HaCaT-TWIST were cultured as previously
436 described.
437
438 **Western blot**
439 Cells were washed with DPBS (Gibco 14190250) and lysed in RIPA buffer (Thermo Scientific
440 89901) with the addition of protease and phosphatase inhibitors (Thermo Scientific 78440).
441 Lysates were centrifuged at 13,000g at 4 °C and quantified using the Pierce BCA Protein Assay
442 Kit (Pierce 23227). Samples were reduced with the laemmli SDS-sample buffer (Boston
443 BioProducts BP111R) and boiled for 10 minutes. For gel electrophoresis, samples were loaded
444 into 4-15% precast protein gels (Bio-Rad 4561084), then transferred to 0.2μm nitrocellulose
445 membranes (Bio-Rad 1704158). Membranes were washed in TBST and blocked with 5% milk in
446 TBST (Boston BioProducts P1400) for 1 hour at RT. Membranes were washed and incubated
447 with primary antibodies overnight. Antibodies used includes Twist (Abcam ab50887) and beta-
448 actin (CST 3700S). On the next day, membranes were washed with TBST and incubated with
449 appropriate secondary antibodies for 1 hour. Blots were incubated with the Immobilon Western
450 Chemiluminescent HRP Substrate (Millipore WBKLS0500) and imaged with the Amersham
451 ImageQuant 800.
452
453 **Immunofluorescence**

454 Cells were cultured on chamber slides (Thermo Scientific 154739) overnight at standard cell
455 culture conditions. Culture media was washed with DPBS (Gibco 14190250) and fixed with 2%
456 PFA in PBS (Santa Cruz 281692) for 15 minutes at RT. Cells were washed with DPBS and
457 permeabilized with 0.1% Triton-X 100 (Thermo Scientific 85111) in PBS, then blocked with 10%
458 goat serum (Thermo Fisher 50062Z) for 1 hour at RT. Primary antibodies used include Twist
459 (Abcam ab50887). Cells were incubated with primary antibody in 10% goat serum overnight at
460 4 °C and washed with DPBS the next day, before incubation with 1:1000 Hoechst 33342
461 (Thermo Fisher H3570) for 1 hour and mounted with VECTASHIELD PLUS Antifade Mounting
462 Medium (Vector Laboratories H1900). Slides were imaged on the Zeiss LSM880 inverted
463 confocal microscope and images were processed using FIJI v1.53.
464
465 **Melanoma infiltration assay**
466 RFP-labeled melanoma cell lines, including A375, SKMEL2, HS294T, were plated on poly-l-
467 lysine coated round glass coverslips (Corning 354085) placed in 24-well plates at 150-200k
468 cells per coverslip. HaCaT cell lines were plated in 6-well plates at 250-300k cells per well. Cells
469 were allowed to attach overnight and the coverslip containing melanoma cells is transferred to
470 6-wells containing HaCaT cell lines using tweezers. All coverslips were placed in the center of
471 the well. KC-melanoma co-cultures were incubated in standard cell culture conditions for 24
472 hours. Co-cultures were imaged by fluorescence microscopy at 4 locations of each coverslip:
473 top, right, bottom and left, to capture variations in melanoma cell infiltration into KC lines. FIJI
474 v1.53 was used to count the number of infiltrating melanoma cells per image and average
475 infiltrating melanoma cells were calculated per well. All experiments were performed in 3 sets,
476 with 3 replicates per set per condition. Average infiltrating cell numbers per well were
477 normalized to the average infiltrating cell number per well in the HaCaT-CTRL condition.
478
479 **scRNA-sequencing analysis of zebrafish Melanoma**

480 Six zebrafish, three each from CTRL and TWIST conditions at 26 weeks post-injection were
481 selected for scRNA-sequencing of melanoma tumors. To account for set differences, one fish
482 from each of three injection sets were chosen in each condition. Melanoma and adjacent skin
483 were dissected from the fish, then enzymatically and mechanically dissociated into single cell
484 solutions as described above. The samples were FACS sorted for GFP and RFP positivity,
485 corresponding to eGFP expressed by keratinocytes and tdTomato expressed by melanoma.
486 The sorted cells were placed in (Gibco 11965) supplemented with 10% FBS (Gemini Bio) and
487 1% penicillin-streptomycin-glutamine. To enrich for keratinocytes, sorted keratinocytes and
488 melanoma cells from each fish was recombined at a 7:3 KC:melanoma ratio. Sorted cells were
489 pelleted and resuspended in DPBS + 0.1% BSA. Samples were also combined based on their
490 genetic perturbation condition. Droplet-based scRNA-seq was performed using the Chromium
491 Single Cell 3′ Library and Gel Bead Kit v3 (10X Genomics) and Chromium Single Cell 3′ Chip G
492 (10X Genomics). 10,000 cells were targeted for encapsulation. GEM generation and library
493 preparation was performed according to kit instructions. Libraries were sequenced on a
494 NovaSeq S4 flow cell. Resulting reads were aligned to the GRCz11 reference genome with the
495 addition of eGFP and tdTomato sequences using CellRanger v5.0.1 (10x Genomics). scRNA-
496 sequencing analysis was performed as detailed above. In addition, melanoma cells were scored
497 using AddModuleScore to assess their enrichment of genes associated with the four main
498 melanoma cell states and intermediate states[28]. The highest scoring gene module for each cell
499 was annotated as its cell state. CellChat[29] was used to analyze cell-cell communication between
500 KC and melanoma clusters using its zebrafish L-R database.
501
502 **Statistics and reproducibility**
503 Statistical analysis and figures were generated by GraphPad Prism 9, R Studio 4.2.0 and
504 Biorender.com. Image processing were performed in FIJI v1.53. Statistical tests are described
505 in figure legends and methods. Experiments were repeated at least three times unless

506 otherwise noted. All animal and cell experiments were performed with a reasonable number of
507 replicates by power calculations or feasibility of the experimental method.
508

509 **Acknowledgements**

510 We thank the MSKCC Single Cell Analytics Innovation Lab for their consult with single cell RNA-
511 sequencing, the MSKCC Molecular Cytology Core Facility for assistance with imaging, the
512 MSKCC Aquatics Core Facility for zebrafish care and maintenance, and the MSKCC Flow
513 Cytometry Core Facility for assistance with FACS. We also thank the members of the White Lab
514 for helpful discussions. YM was supported by a Medical Scientist Training Program (MSTP)
515 grant from the National Institute of General Medical Sciences of the National Institutes of Health
516 (NIH) under award number T32GM152349 to the Weill Cornell/Rockefeller/Sloan Kettering Tri-
517 Institutional MD-PhD Program, the Kirschstein-NRSA predoctoral fellowship (F30) from the
518 National Cancer Institute (NCI) of the NIH under award number F30CA265124, and the Barbara
519 and Stephen Friedman Pre-doctoral Fellowship from MSKCC. MT was support by the Marie-
520 Josée Kravis Women in Science Endeavor Postdoctoral Fellowship and the Experimental
521 Immuno-Oncology Scholars Fellowship. MVH was funded by a K99/R00 Pathway to
522 Independence Award from the NCI(1K99CA266931), the Scholarship for the Next Generation of
523 Scientists from the Cancer Research Society, and a postdoctoral fellowship from the Canadian
524 Institutes of Health Research. EM was supported by the NIH Individual Predoctoral to
525 Postdoctoral Fellow Transition Award under award number 5K00CA223016. JMW was
526 supported by the F30 fellowship from the NCI of the NIH under award number F30CA236442, a
527 predoctoral fellowship (T32) by the Cell and Developmental Biology Program at Weill Cornell
528 Graduate School supported by the NIH under award number T32GM008539, and a MSTP grant
529 from the NIH under award number T32GM007739. RMW was funded through the NIH/NCI
530 Cancer Center Support Grant P30 CA008748, the Melanoma Research Alliance, NIH Research

Program Grants R01CA229215 and R01CA238317, NIH Director's New Innovator Award DP2CA186572, The American Cancer Society, The Alan and Sandra Gerry Metastasis Research Initiative at the Memorial Sloan Kettering Cancer Center, The Harry J. Lloyd Foundation, and Oxford Ludwig Cancer Research.

References

1. Lee, J. T. & Herlyn, M. Microenvironmental influences in melanoma progression. *Journal of Cellular Biochemistry* **101**, 862–872 (2007).
2. Fitzpatrick, T. B. & Breathnach, A. S. The Epidermal Melanin Unit System. *Dermatologische Wochenschrift* **147**, 481–9 (1963).
3. Kunisada, T. *et al.* Transgene expression of steel factor in the basal layer of epidermis promotes survival, proliferation, differentiation and migration of melanocyte precursors. *Development* **125**, 2915–2923 (1998).
4. Tanimura, S. *et al.* Hair Follicle Stem Cells Provide a Functional Niche for Melanocyte Stem Cells. *Cell Stem Cell* **8**, 177–187 (2011).
5. Tang, A. *et al.* E-cadherin is the major mediator of human melanocyte adhesion to keratinocytes in vitro. *Journal of Cell Science* **107**, 983–992 (1994).
6. Imokawa, G., Yada, Y. & Miyagishi, M. Endothelins secreted from human keratinocytes are intrinsic mitogens for human melanocytes. *Journal of Biological Chemistry* **267**, 24675–24680 (1992).
7. Valyi-Nagy, I. T. *et al.* Undifferentiated keratinocytes control growth, morphology, and antigen expression of normal melanocytes through cell-cell contact. *Laboratory Investigation* **69**, 152–159 (1993).

554 8. Shih, I. M., Elder, D. E., Hsu, M. Y. & Herlyn, M. Regulation of Mel-CAM/MUC18 expression
555 on melanocytes of different stages of tumor progression by normal keratinocytes. *Am J*
556 *Pathol* **145**, 837–845 (1994).
557 9. Hara, M., Yaar, M. & Gilchrest, B. A. Endothelin-1 of Keratinocyte Origin Is a Mediator of
558 Melanocyte Dendricity. *Journal of Investigative Dermatology* **105**, 744–748 (1995).
559 10. Hsu, M. Y., Wheelock, M. J., Johnson, K. R. & Herlyn, M. Shifts in cadherin profiles between
560 human normal melanocytes and melanomas. *J Investig Dermatol Symp Proc* **1**, 188–194
561 (1996).
562 11. Hsu, M. Y. *et al.* E-cadherin expression in melanoma cells restores keratinocyte-mediated
563 growth control and down-regulates expression of invasion-related adhesion receptors.
564 *American Journal of Pathology* **156**, 1515–1525 (2000).
565 12. Li, G., Satyamoorthy, K. & Herlyn, M. N-cadherin-mediated intercellular interactions promote
566 survival and migration of melanoma cells. *Cancer Research* **61**, 3819–3825 (2001).
567 13. Fukunaga-Kalabis, M. *et al.* CCN3 controls 3D spatial localization of melanocytes in the
568 human skin through DDR1. *Journal of Cell Biology* **175**, 563–569 (2006).
569 14. Fukunaga-Kalabis, M. *et al.* Downregulation of CCN3 expression as a potential mechanism
570 for melanoma progression. *Oncogene* **27**, 2552–2560 (2008).
571 15. Mescher, M. *et al.* The epidermal polarity protein Par3 is a non-cell autonomous suppressor
572 of malignant melanoma. *Journal of Experimental Medicine* **214**, 339–358 (2017).
573 16. Jamal, S. & Schneider, R. J. UV-induction of keratinocyte endothelin-1 downregulates E-
574 cadherin in melanocytes and melanoma cells. *J Clin Invest* **110**, 443–452 (2002).
575 17. Kim, I. S. *et al.* Microenvironment-derived factors driving metastatic plasticity in melanoma.
576 *Nature Communications* **8**, 14343 (2017).
577 18. Tagore, M. *et al.* GABA Regulates Electrical Activity and Tumor Initiation in Melanoma.
578 *Cancer Discovery* **13**, 2270–2291 (2023).

579 19. Callahan, S. J. *et al.* Cancer modeling by Transgene Electroporation in Adult Zebrafish
580 (TEAZ). *Disease Models & Mechanisms* **11**, dmm034561 (2018).
581 20. Kaufman, C. K. *et al.* A zebrafish melanoma model reveals emergence of neural crest
582 identity during melanoma initiation. *Science* **351**, aad2197–aad2197 (2016).
583 21. Li, Q. & Uitto, J. Zebrafish as a Model System to Study Skin Biology and Pathology. *Journal*
584 *of Investigative Dermatology* **134**, 1–6 (2014).
585 22. Gong, Z. *et al.* Green fluorescent protein expression in germ-line transmitted transgenic
586 zebrafish under a stratified epithelial promoter from keratin8. *Developmental Dynamics* **223**,
587 204–215 (2002).
588 23. Montal, E., Suresh, S., Ma, Y., Tagore, M. M. & White, R. M. Cancer Modeling by
589 Transgene Electroporation in Adult Zebrafish (TEAZ). in *Zebrafish: Methods and Protocols*
590 (eds. Amatruda, J. F., Houart, C., Kawakami, K. & Poss, K. D.) 83–97 (Springer US, New
591 York, NY, 2024). doi:10.1007/978-1-0716-3401-1_5.
592 24. Haensel, D. & Dai, X. Epithelial-to-mesenchymal transition in cutaneous wound healing:
593 Where we are and where we are heading. *Developmental Dynamics* **247**, 473–480 (2018).
594 25. Leopold, P. L., Vincent, J. & Wang, H. A comparison of epithelial-to-mesenchymal transition
595 and re-epithelialization. *Seminars in Cancer Biology* **22**, 471–483 (2012).
596 26. Moreno-Bueno, G. *et al.* The morphological and molecular features of the epithelial-to-
597 mesenchymal transition. *Nature Protocols* **4**, 1591–1613 (2009).
598 27. Hunter, M. V., Moncada, R., Weiss, J. M., Yanai, I. & White, R. M. Spatially resolved
599 transcriptomics reveals the architecture of the tumor-microenvironment interface. *Nature*
600 *Communications 2021 12:1* **12**, 1–16 (2021).
601 28. Tsoi, J. *et al.* Multi-stage Differentiation Defines Melanoma Subtypes with Differential
602 Vulnerability to Drug-Induced Iron-Dependent Oxidative Stress. *Cancer Cell* **33**, 890-904.e5
603 (2018).

604 29. Jin, S. *et al.* Inference and analysis of cell-cell communication using CellChat. *Nature*
605 *communications* **12**, 1088 (2021).
606 30. Eom, D. S., Patterson, L. B., Bostic, R. R. & Parichy, D. M. Immunoglobulin superfamily
607 receptor Junctional adhesion molecule 3 (Jam3) requirement for melanophore survival and
608 patterning during formation of zebrafish stripes. *Developmental Biology* **476**, 314–327
609 (2021).
610 31. Arcangeli, M. L. *et al.* The Junctional Adhesion Molecule-B regulates JAM-C-dependent
611 melanoma cell metastasis. *FEBS Letters* **586**, 4046–4051 (2012).
612 32. Langer, H. F. *et al.* A novel function of junctional adhesion molecule-C in mediating
613 melanoma cell metastasis. *Cancer Research* **71**, 4096–4105 (2011).
614 33. Tissue expression of F11R - Staining in skin. *The Human Protein Atlas*
615 https://www.proteinatlas.org/ENSG00000158769-F11R/tissue/skin.
616 34. Tissue expression of JAM3 - Staining in skin. *The Human Protein Atlas*
617 https://www.proteinatlas.org/ENSG00000166086-JAM3/tissue/skin.
618 35. Koike, Y., Yozaki, M., Utani, A. & Murota, H. Fibroblast growth factor 2 accelerates the
619 epithelial–mesenchymal transition in keratinocytes during wound healing process. *Sci Rep*
620 **10**, 18545 (2020).
621 36. Halaban, R., Kwon, B. S., Ghosh, S., Delli Bovi, P. & Baird, A. bFGF as an autocrine growth
622 factor for human melanomas. *Oncogene Res* **3**, 177–186 (1988).
623 37. Hoek, K. S. *et al.* Metastatic potential of melanomas defined by specific gene expression
624 profiles with no BRAF signature. *Pigment Cell Research* **19**, 290–302 (2006).
625 38. Hu, F. *et al.* Sortilin-Mediated Endocytosis Determines Levels of the Frontotemporal
626 Dementia Protein, Progranulin. *Neuron* **68**, 654–667 (2010).
627 39. Daniel, R., He, Z., Carmichael, K. P., Halper, J. & Bateman, A. Cellular Localization of Gene
628 Expression for Progranulin. *J Histochem Cytochem.* **48**, 999–1009 (2000).

629 40. Shoyab, M., McDonald, V. L., Byles, C., Todaro, G. J. & Plowman, G. D. Epithelins 1 and 2:
630 isolation and characterization of two cysteine-rich growth-modulating proteins. *Proceedings*
631 *of the National Academy of Sciences* **87**, 7912–7916 (1990).
632 41. He, Z., Ong, C. H. P., Halper, J. & Bateman, A. Progranulin is a mediator of the wound
633 response. *Nature Medicine* **9**, 225–229 (2003).
634 42. Tanimoto, R. *et al.* The perlecan-interacting growth factor progranulin regulates
635 ubiquitination, sorting, and lysosomal degradation of sortilin. *Matrix Biol* **64**, 27–39 (2017).
636 43. Truzzi, F. *et al.* Neurotrophins and Their Receptors Stimulate Melanoma Cell Proliferation
637 and Migration. *Journal of Investigative Dermatology* **128**, 2031–2040 (2008).
638 44. White, R. M. *et al.* Transparent Adult Zebrafish as a Tool for In Vivo Transplantation
639 Analysis. *Cell Stem Cell* **2**, 183–189 (2008).
640 45. Kwan, K. M. *et al.* The Tol2kit: A multisite gateway-based construction kit for Tol2
641 transposon transgenesis constructs. *Developmental Dynamics* **236**, 3088–3099 (2007).
642 46. Montal, E., Lumaquin, D., Ma, Y., Suresh, S. & White, R. M. Modeling the effects of genetic-
643 and diet-induced obesity on melanoma progression in zebrafish. *Disease Models* \&
644 *Mechanisms* **16**, dmm049671 (2023).
645 47. Butler, A., Hoffman, P., Smibert, P., Papalexi, E. & Satija, R. Integrating single-cell
646 transcriptomic data across different conditions, technologies, and species. *Nat Biotechnol*
647 **36**, 411–420 (2018).
648 48. Hao, Y. *et al.* Integrated analysis of multimodal single-cell data. *Cell* **184**, 3573-3587.e29
649 (2021).
650 49. Hu, Y. *et al.* An integrative approach to ortholog prediction for disease-focused and other
651 functional studies. *BMC Bioinformatics* **12**, 357 (2011).
652 50. Campbell, N. R. *et al.* Cooperation between melanoma cell states promotes metastasis
653 through heterotypic cluster formation. *Developmental Cell* **56**, 2808-2825.e10 (2021).

654 51. Subramanian, A. *et al.* Gene set enrichment analysis: A knowledge-based approach for
655 interpreting genome-wide expression profiles. *Proceedings of the National Academy of*
656 *Sciences of the United States of America* **102**, 15545–15550 (2005).
657 52. Liberzon, A. *et al.* The Molecular Signatures Database Hallmark Gene Set Collection. *Cell*
658 *Systems* **1**, 417–425 (2015).
659

Figure 1

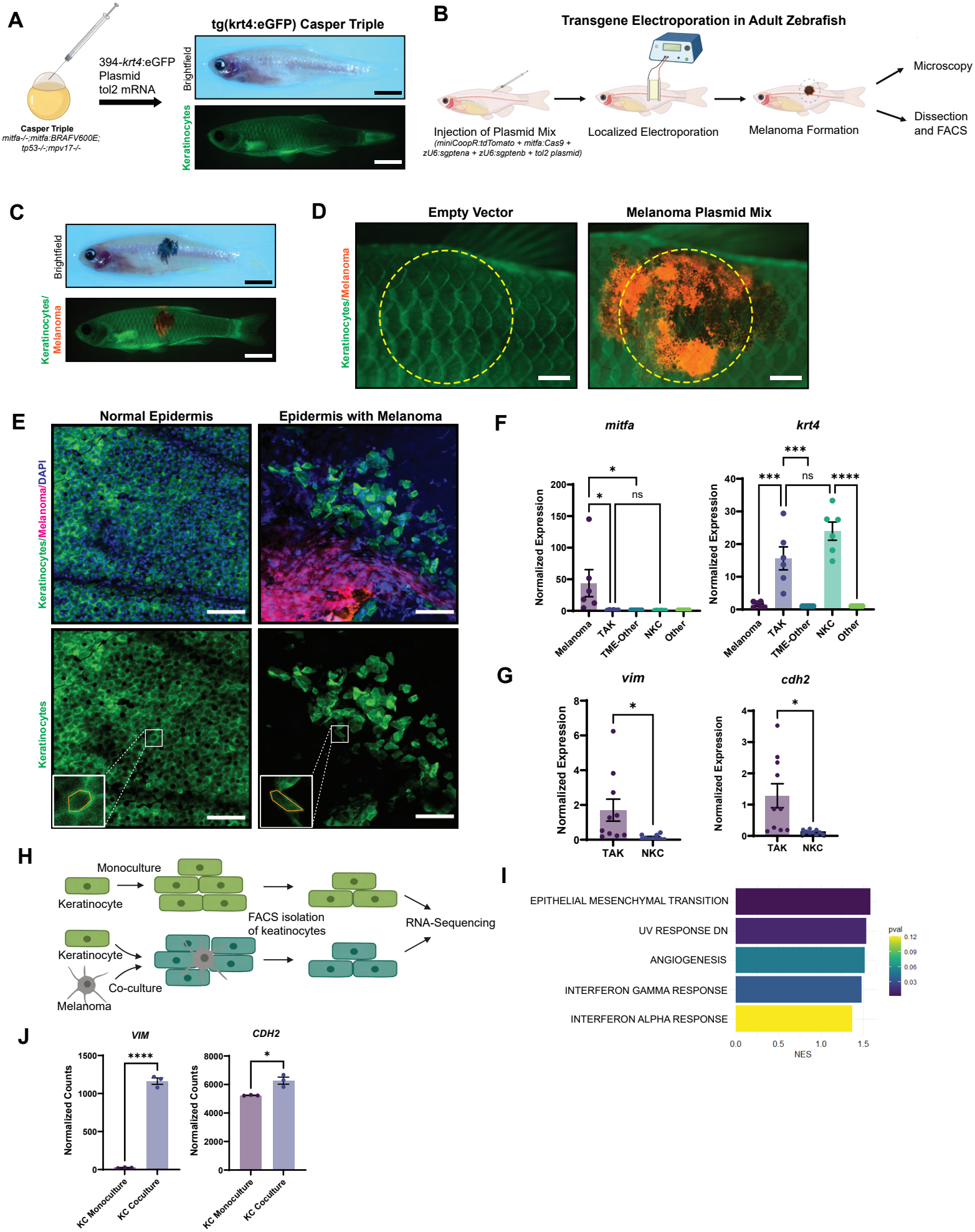
A
394-krt4:eGFP
Plasmid
tol2 mRNA
Casper Triple
mitfa-/-;mitfa:BRAFV600E;
tp53-/-;mpv17-/-
tg(krt4:eGFP) Casper Triple
Brightfield
Keratinocytes
B
Transgene Electroporation in Adult Zebrafish
Injection of Plasmid Mix
(miniCoopR:tdTomato + mitfa:Cas9 +
zU6:sgptena + zU6:sgptenb + tol2 plasmid)
Localized Electroporation
Melanoma Formation
Microscopy
Dissection
and FACS
C
Brightfield
Keratinocytes/
Melanoma
D
Empty Vector
Melanoma Plasmid Mix
Keratinocytes/Melanoma
E
Normal Epidermis
Epidermis with Melanoma
Keratinocytes/Melanoma/DAPI
Keratinocytes
F
mitfa
krt4
Normalized Expression
Melanoma
TAK
TME-Other
NKC
Other
ns
G
vim
cdh2
Normalized Expression
TAK
NKC
H
Monoculture
Keratinocyte
FACS isolation
of keatinocytes
RNA-Sequencing
Co-culture
Melanoma
I
EPITHELIAL MESENCHYMAL TRANSITION
UV RESPONSE DN
ANGIOGENESIS
INTERFERON GAMMA RESPONSE
INTERFERON ALPHA RESPONSE
NES
pval
J
VIM
CDH2
Normalized Counts
KC Monoculture
KC Coculture

Figure 1. Keratinocytes in the melanoma microenvironment undergo EMT-like changes.

(A) Generation of transparent zebrafish with GFP-labeling of keratinocytes. Casper Triples (*mitfa-/-;mitfa:*BRAFV600E;*tp53-/-;mpv17-/-*) were injected with the Tol2Kit 394 vector containing a *krt4*:eGFP cassette and tol2 mRNA. Brightfield shows a transparent zebrafish while fluorescence imaging shows eGFP-labeling of keratinocytes. (Scale bar = 5mm)

(B) Schematic of TEAZ (Transgene Electroporation in Adult Zebrafish). Plasmid mix containing miniCoopR:tdTomato, *mitfa:*Cas9, *zU6:sgptena*, *zU6:sgptenb*, and the tol2 plasmid was injected superficially in the flank of the zebrafish. Electroporation of the injection site results in rescue of melanocyte precursors and the generation of a localized melanoma that could be analyzed by microscopy and FACS.

(C) Brightfield and immunofluorescence of zebrafish 8-weeks post-TEAZ with localized and fluorescently labeled melanoma. (Scale bar = 5mm)

(D) Immunofluorescence imaging of TEAZ region after 8-weeks, comparing empty vector control vs. miniCoopR:tdT conditions, with yellow dotted circles indicating general area of dissection for FACS. (Scale bar = 1mm)

(E) Confocal imaging of zebrafish epidermis. Normal epidermis of Tg(*krt4:*eGFP) Casper Triple post-TEAZ with empty vector control shows eGFP-labeled, polygonal shaped keratinocytes regularly connected while epidermis with melanoma generated with *miniCoopR*-drived melanocyte rescue shows disrupted epidermis and irregularly shaped keratinocytes. (Scale bar = 50um)

(F) qPCR of FACS sorted zebrafish epidermis with or without melanoma. tdTomato-labeled melanoma cells, eGFP-labeled keratinocytes and non-fluorescently labeled TME cells were isolated by dissection (as indicated in G) and FACS. Comparison of *mitfa* and *krt4* expression of samples normalized to non-fluorescent cells, either ‘TME-Other’ in tumor

samples or ‘Other’ in non-tumor samples, shows enrichment of *mitfa* in melanoma sample and *krt4* in keratinocyte sample. ns is non-significant, * is $p \leq 0.05$, *** is $p \leq 0.001$, **** is $p \leq 0.0001$ by Tukey’s multiple comparisons test.

(G) Comparison of the EMT-markers *vim* and *cdh2* shows enrichment in TME keratinocytes vs. keratinocytes from epidermis without melanoma. * is $p \leq 0.05$ by Welch’s t-test.

(H) Schematic of keratinocyte-melanoma co-culture experiment. HaCaTs were cultured in monoculture or co-culture with A375 melanoma cells in triplicates for 21 days, followed by FACS isolation of keratinocytes for RNA-sequencing comparing co-culture vs. monoculture keratinocytes.

(I) Top 5 enriched Hallmark pathways in HaCaTs co-cultured with A375 melanoma cells compared with HaCaTs in monoculture.

(J) Normalized counts of EMT biomarkers vimentin (*VIM*) and N-cadherin (*CDH2*).

Figure 2

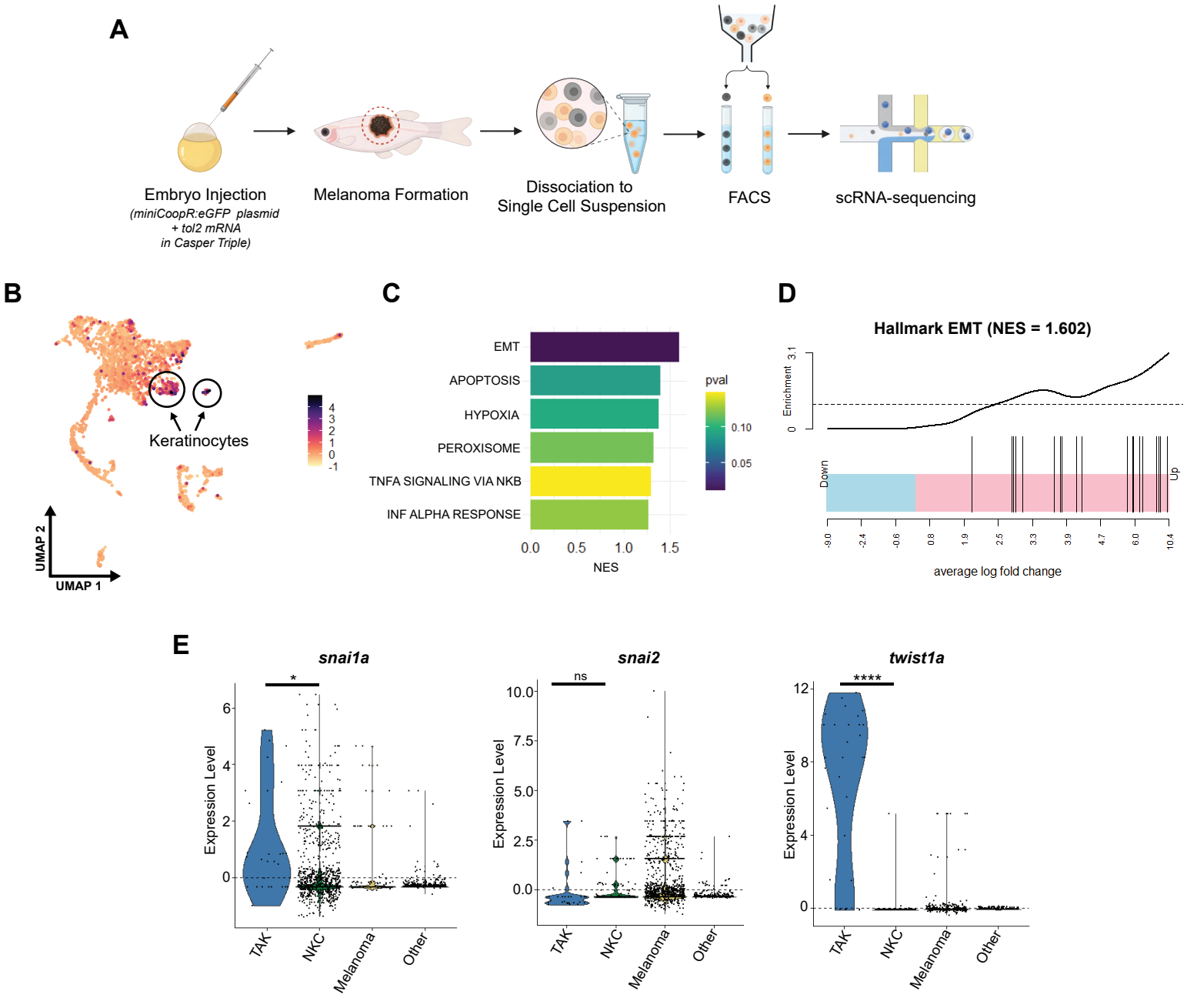
A
Embryo Injection
(miniCoopR:eGFP plasmid
+ tol2 mRNA
in Casper Triple)
Melanoma Formation
Dissociation to
Single Cell Suspension
FACS
scRNA-sequencing
B
Keratinocytes
UMAP 2
UMAP 1
C
EMT
APOPTOSIS
HYPOXIA
PEROXISOME
TNFA SIGNALING VIA NKB
INF ALPHA RESPONSE
NES
pval
D
Hallmark EMT (NES = 1.602)
Enrichment
Down
Up
average log fold change
E
snai1a
snai2
twist1a
Expression Level
TAK
NKC
Melanoma
Other

Figure 2. Zebrafish scRNA-sequencing shows upregulation of EMT-TFs in tumor-associated keratinocytes.

(A) Schematic of scRNA-sequencing experiment. Embryo injection with miniCoopR:eGFP plasmid and tol2 mRNA in Casper Triples (*mitfa-/-;mitfa:*BRAFV600E;*tp53-/-;mpv17-/-*) results in melanocyte rescue and subsequent melanoma formation. Melanoma was dissected and dissociated to single cell suspension for FACS isolation of eGFP+ melanoma cells and non-fluorescent TME cells for single cell RNA-sequencing.

(B) Dimensionality reduction and subsequent analysis with zebrafish keratinocyte gene module scoring highlights two keratinocyte clusters.

(C) Top 6 GSEA Hallmark pathways enriched in comparison between keratinocyte clusters.

(D) Hallmark EMT pathway enrichment in keratinocyte clusters.

(E) Expression of EMT-transcription factors Snail (*snai1a*), Slug (*snai2*), and Twist1 (*twist1a*) in TAK vs. NKC, Melanoma, and Other TME cells. ns is no significance, * is $p \leq 0.05$, **** is $p \leq 0.0001$.

Figure 3

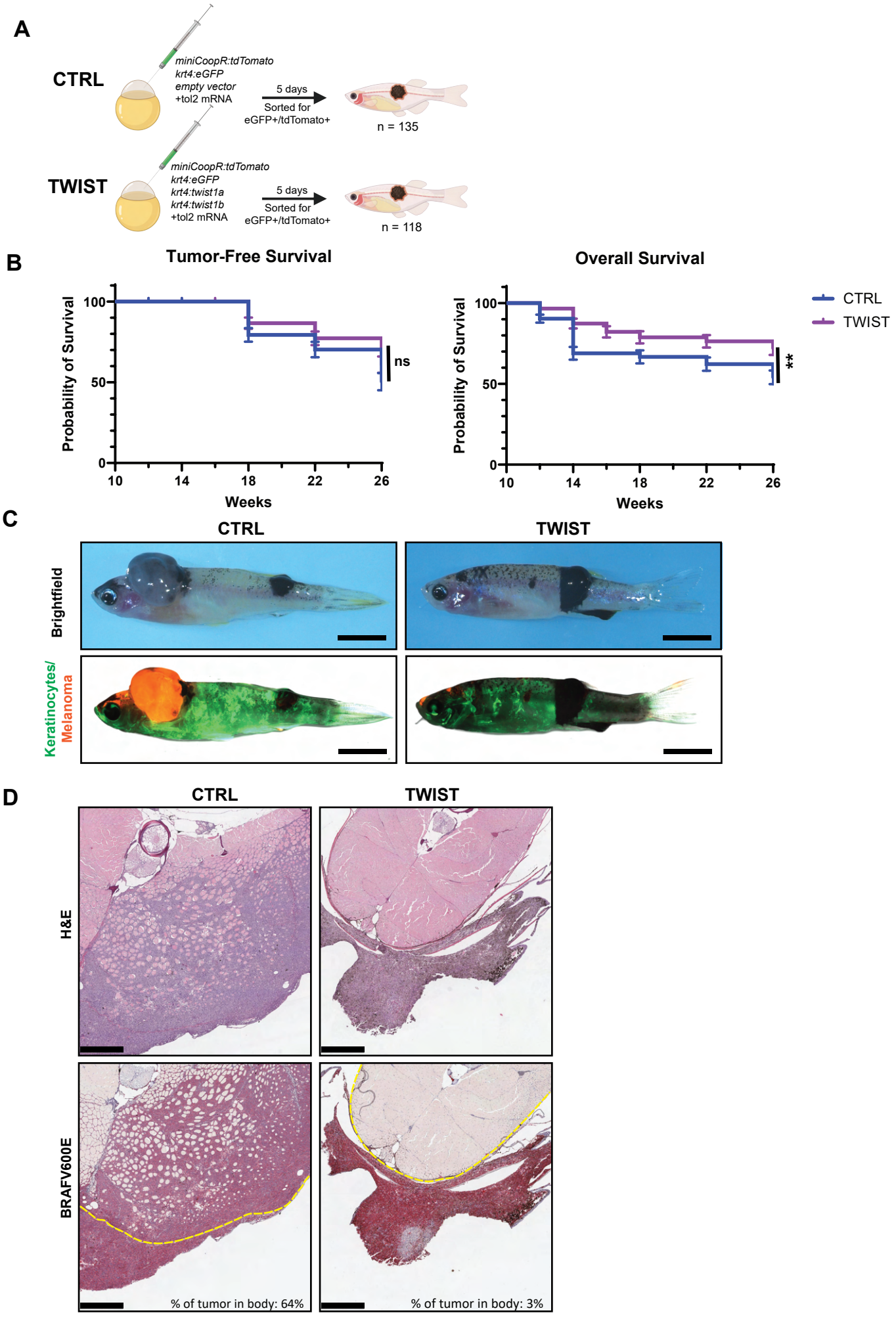
A
CTRL
miniCoopR:tdTomato
krt4:eGFP
empty vector
+tol2 mRNA
5 days
Sorted for
eGFP+/tdTomato+
n = 135
TWIST
miniCoopR:tdTomato
krt4:eGFP
krt4:twist1a
krt4:twist1b
+tol2 mRNA
5 days
Sorted for
eGFP+/tdTomato+
n = 118
B
Tumor-Free Survival
Overall Survival
Probability of Survival
100
50
0
10
14
18
22
26
Weeks
ns
**
CTRL
TWIST
C
CTRL
TWIST
Brightfield
Keratinocytes/
Melanoma
D
CTRL
TWIST
H&E
BRAFV600E
% of tumor in body: 64%
% of tumor in body: 3%

Figure 3. Overexpression of twist1a/b results in improved survival of fish with melanoma.

(A) Schematic of zebrafish melanoma model with labeling and perturbation of keratinocytes. *Twist1a* and *twist1b* are overexpressed under the keratinocyte-specific *krt4* promoter in the TWIST condition and an empty vector control was used in the CTRL condition. Plasmid mix containing miniCoopR-tdTomato, *krt4*:eGFP, either empty vector or *krt4:twist1a/b*, with tol2 mRNA were injected into Casper Triples (*mitfa-/-;mitfa:*BRAFV600E;*tp53-/-;mpv17-/-*). Fish were sorted at 5 days for eGFP and tdTomato positivity as marker of successful keratinocyte labeling and melanocyte rescue.

(B) Tumor-free survival and overall survival of A. ns is no significance, ** is $p \leq 0.01$ by Log-rank (Mantel-Cox) test.

(C) Sample images of zebrafish with melanoma at 26 weeks post-injection. Melanomas are pigmented in brightfield images. Keratinocytes are labeled by eGFP and melanoma are labeled by tdTomato in fluorescence images. Scale bar = 5mm.

(D) H&E and IHC of cross-sections through zebrafish body and melanoma. Dotted yellow line demarcates border of body. Percent of tumor in body is calculated as tumor area within body border divided by total tumor area. Scale bar = 500um.

Figure 4

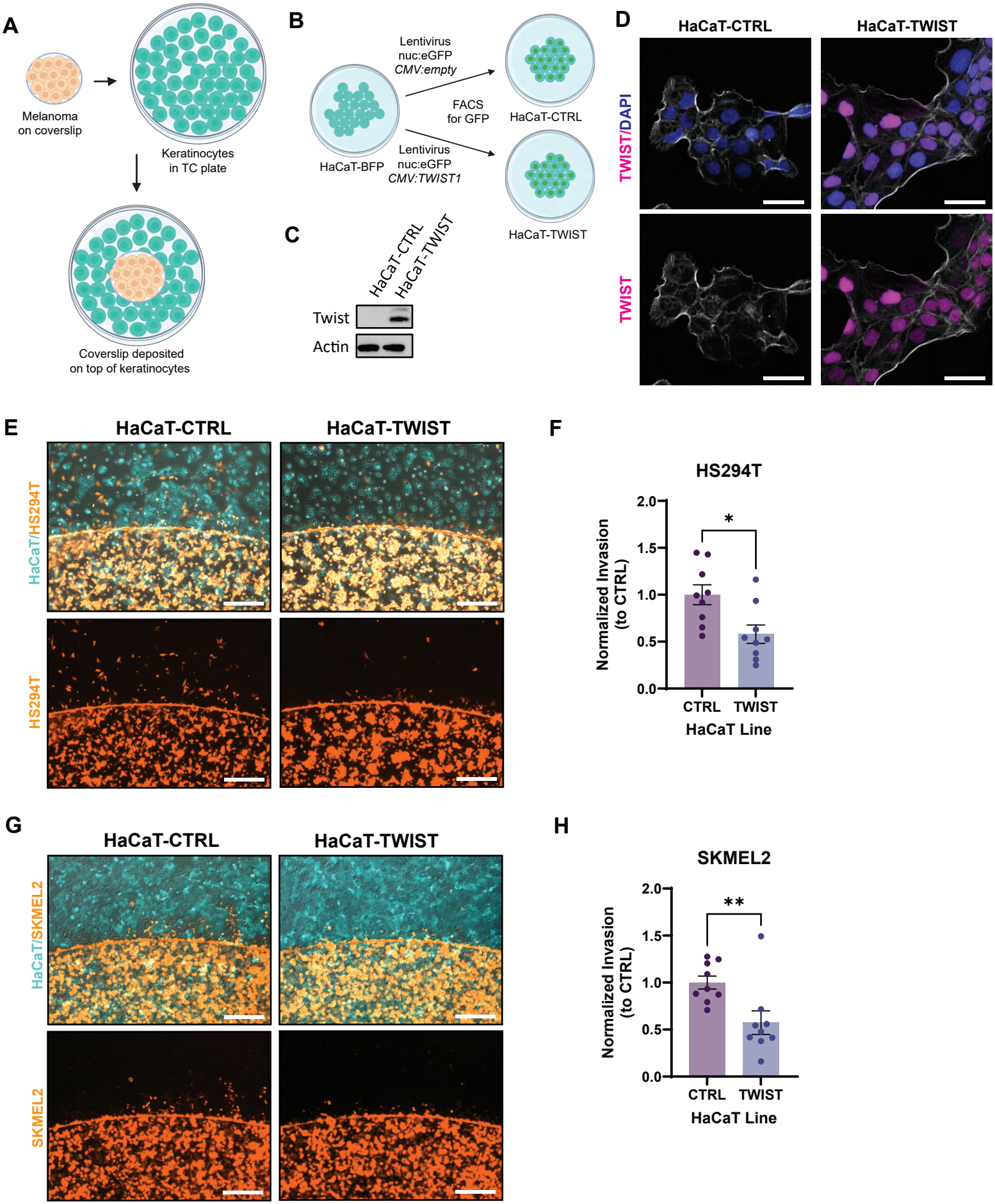
A
Melanoma on coverslip
Keratinocytes in TC plate
Coverslip deposited on top of keratinocytes
B
HaCaT-BFP
Lentivirus nuc:eGFP CMV:empty
FACS for GFP
HaCaT-CTRL
Lentivirus nuc:eGFP CMV:TWIST1
HaCaT-TWIST
C
HaCaT-CTRL
HaCaT-TWIST
Twist
Actin
D
HaCaT-CTRL
HaCaT-TWIST
TWIST/DAPI
TWIST
E
HaCaT-CTRL
HaCaT-TWIST
HaCaT/HS294T
HS294T
F
HS294T
Normalized Invasion (to CTRL)
2.0
1.5
1.0
0.5
0.0
*
CTRL
TWIST
HaCaT Line
G
HaCaT-CTRL
HaCaT-TWIST
HaCaT/SKMEL2
SKMEL2
H
SKMEL2
Normalized Invasion (to CTRL)
2.0
1.5
1.0
0.5
0.0
**
CTRL
TWIST
HaCaT Line

Figure 4. Zebrafish findings are recapitulated in human cell lines.

(A) Schematic of coverslip cell infiltration assay. Melanoma cells are plated on a coverslip and allowed to attach overnight. The coverslip is then transferred into a well of keratinocytes to assess melanoma infiltration into keratinocytes.

(B) Generation of a HaCaT cell line overexpressing *TWIST1*. HaCaT-BFP was infected with lentivirus containing cassette with nuclear localized GFP and *CMV* driven *TWIST1* or no ORF. Infected cell lines were allowed to grow for a week before sorting for nuclear GFP as a marker of successful integration.

(C) Western blot for Twist expression in HaCaT-CTRL and HaCaT-TWIST.

(D) Immunofluorescence imaging for Twist localization in HaCaT-CTRL and HaCaT-TWIST. TWIST staining is pseudo-colored in magenta, DAPI in blue, phalloidin in white. Scale bar = 50um.

(E) Immunofluorescence imaging of coverslip cell infiltration assay after 20 hours with HS294T-tdT (orange) melanoma cells in co-culture with either HaCaT-CTRL or HaCaT-TWIST (cyan). Scale bar = 500um.

(F) Quantification of E. Infiltrating HS294T melanoma cells from each image were counted and averaged across four images per well. Resulting cell counts were normalized to average cell counts of HaCaT-CTRL from each set. N = 9, 3 sets, 3 replicates/wells per set. * is $p \leq 0.05$ by t-test.

(G) Immunofluorescence imaging of coverslip cell infiltration assay after 20 hours with SKMEL2-tdT (orange) melanoma cells in co-culture with either HaCaT-CTRL or HaCaT-TWIST (cyan). Scale bar = 500um.

(H) Quantification of G. Infiltrating SKMEL2 melanoma cells from each image were counted and averaged across four images per well. Resulting cell counts were normalized to

average cell counts of HaCaT-CTRL from each set. N = 9, 3 sets, 3 replicates/wells per set. ** is $p \leq 0.01$ by t-test.

Figure 5

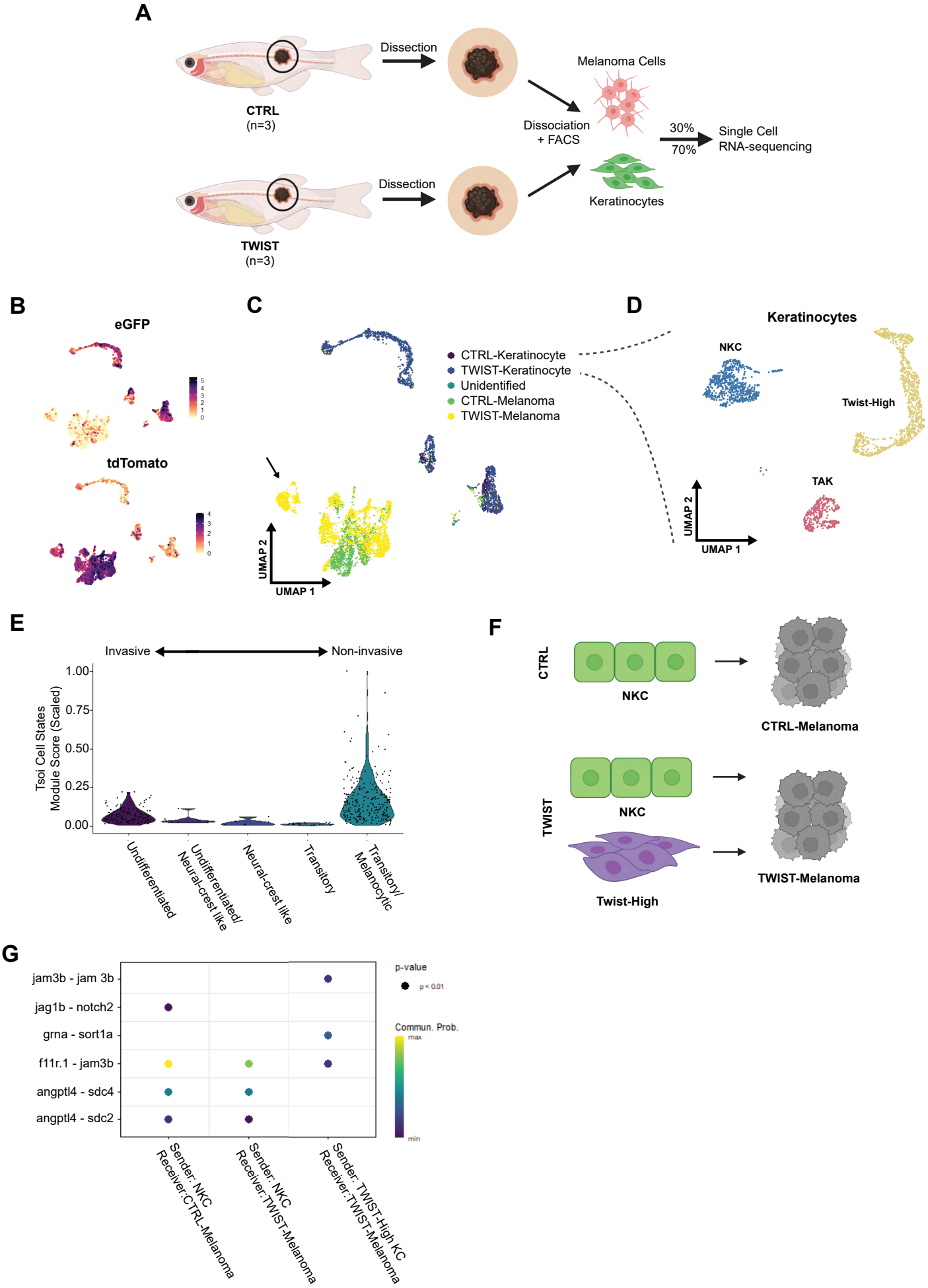
A
Dissection
CTRL
(n=3)
Melanoma Cells
Dissociation
+ FACS
30%
70%
Single Cell
RNA-sequencing
Dissection
TWIST
(n=3)
Keratinocytes
B
eGFP
tdTomato
C
CTRL-Keratinocyte
TWIST-Keratinocyte
Unidentified
CTRL-Melanoma
TWIST-Melanoma
UMAP 2
UMAP 1
D
Keratinocytes
NKC
Twist-High
TAK
UMAP 2
UMAP 1
E
Invasive
Non-invasive
Tsoi Cell States
Module Score (Scaled)
1.00
0.75
0.50
0.25
0.00
Undifferentiated
Undifferentiated/
Neural-crest like
Neural-crest like
Transitory
Transitory/
Melanocytic
F
CTRL
NKC
CTRL-Melanoma
TWIST
NKC
Twist-High
TWIST-Melanoma
G
jam3b - jam 3b
jag1b - notch2
grna - sort1a
f11r.1 - jam3b
angptl4 - sdc4
angptl4 - sdc2
Sender: NKC
Receiver:CTRL-Melanoma
Sender: NKC
Receiver:TWIST-Melanoma
Sender: TWIST-High KC
Receiver:TWIST-Melanoma
p-value
p < 0.01
Commun. Prob.
max
min

Figure 5. scRNA-sequencing shows unique keratinocyte-melanoma communication with twist1a/b overexpression in keratinocytes.

(A) Schematic of scRNA-sequencing protocol. Melanoma and surrounding tissue were dissected from 26-weeks old zebrafish from either CTRL or TWIST conditions as shown in Figure 3. Samples were dissociated to single cell suspensions for FACS isolation of keratinocytes (GFP) and melanoma (tdTomato). Keratinocytes and melanoma were recombined per condition at a ratio of 7:3 for enrichment of keratinocytes for scRNA-sequencing.

(B) UMAP dimensional reduction and feature plots of scRNA-sequencing dataset. CTRL and TWIST samples were sequenced, and cell types were identified using eGFP+ for keratinocytes and tdTomato+ for melanoma, after which the datasets were integrated.

(C) UMAP showing cell type assignments of each cluster within either CTRL or TWIST conditions. Arrow indicates a TWIST-melanoma population clustering separately from other melanoma clusters.

(D) UMAP highlighting keratinocyte clusters, with a Tumor-Associated Keratinocyte (TAK) cluster, a Normal Keratinocyte Cluster (NKC), and a Twist-High cluster unique to the TWIST condition.

(E) Melanoma cell state analysis of the melanoma cluster unique to the Twist condition indicated by arrow in Figure 5C.

(F) Schematic overview of CellChat analysis. In CTRL condition, we analyzed Ligand-Receptor pairs with NKC as sender and CTRL-Melanoma as receiver. In TWIST condition, we analyzed L-R pairs with both NKC and Twist-High as sender and TWIST-Melanoma as receiver.

(G) CellChat analysis results. L-R pairs shown at $p<0.01$, with color scale indicating communication probability of L-R pair.